

An orbital-free molecular dynamics study of melting in K_{20} , K_{55} , K_{92} , K_{142} , Rb_{55} and Cs_{55} clusters.

Andrés Aguado

Departamento de Física Teórica, Universidad de Valladolid, Valladolid 47011, Spain

The melting-like transition in potassium clusters K_N , with $N=20, 55, 92$ and 142 , is studied by using an orbital-free density-functional constant-energy molecular dynamics simulation method, and compared to previous theoretical results on the melting-like transition in sodium clusters of the same sizes. Melting in potassium and sodium clusters proceeds in a similar way: a surface melting stage develops upon heating before the homogeneous melting temperature is reached. Premelting effects are nevertheless more important and more easily established in potassium clusters, and the transition regions spread over temperature intervals which are wider than in the case of sodium. For all the sizes considered, the percentage melting temperature reduction when passing from Na to K clusters is substantially larger than in the bulk. Once those two materials have been compared for a number of different cluster sizes, we study the melting-like transition in Rb_{55} and Cs_{55} clusters and make a comparison with the melting behavior of Na_{55} and K_{55} . As the atomic number increases, the height of the specific heat peaks decreases, their width increases, and the melting temperature decreases as in bulk melting, but in a more pronounced way.

PACS numbers: 36.40.Ei 64.70.Dv

I. INTRODUCTION

The melting transition of a pure bulk material occurs at a well defined temperature for a given external pressure. The melting-like transition in small clusters composed of a finite number of atoms spreads instead over a temperature interval that widens as the cluster size decreases. A number of thermal properties sensitive to the cluster size and essentially different from those found in bulk materials emerge in the transition region defined by that temperature interval, which has motivated a lot of theoretical¹⁻⁸ and experimental⁹⁻¹² investigations. The experiments of Schmidt *et al.*¹⁰ have shown strong non-monotonic variations of the melting temperature of free sodium clusters with size, which can not be completely explained either by electronic or geometric shell closing arguments. The theoretical simulations have predicted the occurrence of several premelting effects, like surface melting or structural isomerizations, and also the existence of a dynamic coexistence regime, where the cluster can fluctuate in time between being completely solid or liquid.

We have previously reported density functional orbital-free molecular dynamics (OFMD) simulations of the melting process in sodium clusters Na_N , with $N=8, 20, 55, 92$, and 142 .^{7,8} The OFMD technique¹³ is completely analogous to the method devised by Car and Parrinello (CP) to perform dynamic simulations at an *ab initio* level,¹⁴ but the electron density is taken as the dynamic variable,¹⁵ as opposed to the Kohn-Sham (KS) orbitals¹⁶ in the original CP method. This technique, whose main advantage over KS-based methods is that the computational effort to update the electronic system scales linearly with cluster size, has been already used both in solid state^{17,18} and cluster^{3,19,20} physics.

Our predictions of the temperatures at which homogeneous cluster melting occurs were in good agreement with the experiments of Haberland's group,^{10,11} excepting the enhancement of the melting temperature around $N=55$, which was not reproduced. We also observed a number of interesting premelting effects, mostly the establishment of a surface melting stage at a temperature lower than the homogeneous melting temperature for Na_{20} , Na_{92} and Na_{142} , and several isomerization transitions in Na_8 and Na_{20} . It is interesting to study similar systems like clusters of K, Rb and Cs in order to assess whether those trends are a general feature of alkali clusters or not. With this goal, we consider in this paper the melting-like transition of K_N clusters, with $N=20, 55, 92$, and 142 , and compare it with that of sodium clusters of the same size. As a second step, for a fixed cluster size of $N=55$, we study the melting behavior of Rb_{55} and Cs_{55} and compare it with that of Na_{55} and K_{55} . In the next section we briefly present some technical details of the method. The results are presented and discussed in section III and, finally, section IV summarizes our main conclusions.

II. THEORY

The orbital-free molecular dynamics method is a Car-Parrinello total energy scheme¹⁴ which uses an explicit kinetic-energy functional of the electron density, and has the electron density as the dynamical variable, as opposed to the KS single particle wavefunctions. The main features of the energy functional and the calculation scheme have been described at length in previous work,^{13,17,19,3,7} and details of our method are as described by Aguado *et al.*⁷ In brief, the electronic kinetic energy functional of the electron density, $n(\vec{r})$, cor-

responds to the gradient expansion around the homogeneous limit through second order^{15,21–23}

$$T_s[n] = T^{TF}[n] + \frac{1}{9}T^W[n], \quad (1)$$

where the first term is the Thomas-Fermi functional (Hartree atomic units have been used)

$$T^{TF}[n] = \frac{3}{10}(3\pi^2)^{2/3} \int n(\vec{r})^{5/3} d\vec{r}, \quad (2)$$

and the second is the lowest order gradient correction, where T^W , the von Weizsäcker term, is given by

$$T^W[n] = \frac{1}{8} \int \frac{|\nabla n(\vec{r})|^2}{n(\vec{r})} d\vec{r}. \quad (3)$$

The local density approximation is used for exchange and correlation.^{24,25} In the external field acting on the electrons, $V_{ext}(\vec{r}) = \sum_n v(\vec{r} - \vec{R}_n)$, we take v to be the local pseudopotential of Fiolhais *et al.*,²⁶ which reproduces well the properties of bulk alkalis and has been shown to have good transferability to alkali clusters.²⁷ The cluster is placed in a unit cell of a cubic superlattice, and the set of plane waves periodic in the superlattice is used as a basis set to expand the valence density. Following Car and Parrinello,¹⁴ the coefficients of that expansion are regarded as generalized coordinates of a set of fictitious classical particles, and the corresponding Lagrange equations of motion for the ions and the electron density distribution are solved as described in Ref. 7.

The calculations used a supercell of edge 71 a.u. for K_{20} and 81 a.u. for K_{55} , K_{92} , K_{142} , Rb_{55} and Cs_{55} . An energy cut-off of 8 Ryd was used in the plane wave expansion of the energy for K clusters, and of 6.15 Ryd for Rb and Cs clusters. In all cases, a $64 \times 64 \times 64$ grid was used. The cut-offs used give a convergence of bond lengths and binding energies as good as that obtained for sodium clusters.⁷ The fictitious mass associated with the electron density coefficients ranged between 6.3×10^8 and 4.0×10^9 a.u., depending on the material and on the temperature of the simulations. The equations of motion of K clusters were integrated using the Verlet algorithm²⁸ for both electrons and ions with a time step ranging from $\Delta t = 0.83 \times 10^{-15}$ sec. for the simulations performed at the lowest temperatures, to $\Delta t = 0.67 \times 10^{-15}$ sec. for those at the highest ones. In the case of Rb_{55} the time steps ranged from $\Delta t = 2.38 \times 10^{-15}$ sec. to $\Delta t = 1.31 \times 10^{-15}$ sec, and in the case of Cs_{55} from $\Delta t = 4.29 \times 10^{-15}$ sec. to $\Delta t = 1.79 \times 10^{-15}$ sec. These choices resulted in a conservation of the total energy better than 0.1 % in all cases.

Several molecular dynamics simulation runs at different constant energies were performed in order to obtain the caloric curve for each cluster. The initial positions of the atoms for the first run were taken by slightly deforming the equilibrium low-temperature geometry of the cluster. The final configuration of each run served as the

starting geometry for the next run at a different energy. The initial velocities for every new run were obtained by scaling the final velocities of the preceding run. The total simulation times for each run at constant energy were 40 ps for K clusters. 80 ps for Rb_{55} , and 140 ps for Cs_{55} . These different simulation times were chosen in order to obtain a good convergence of the several melting indicators described below. They increase with atomic number because the typical atomic vibrational frequencies decrease with atomic number.

A number of indicators to locate the melting-like transition were employed. Namely, the specific heat defined by²⁹

$$C_v = [N - N(1 - \frac{2}{3N-6}) \langle E_{kin} \rangle_t \langle E_{kin}^{-1} \rangle_t]^{-1}, \quad (4)$$

where N is the number of atoms and $\langle \rangle_t$ indicates the average along a trajectory; the root-mean-square (rms) bond length fluctuation¹

$$\delta = \frac{2}{N(N-1)} \sum_{i<j} \frac{(\langle R_{ij}^2 \rangle_t - \langle R_{ij} \rangle_t^2)^{1/2}}{\langle R_{ij} \rangle_t}; \quad (5)$$

the “atomic equivalence indexes”³⁰

$$\sigma_i(t) = \sum_j |\vec{R}_i(t) - \vec{R}_j(t)|, \quad (6)$$

and finally, the average over a whole dynamical trajectory of the radial atomic distribution function $g(r)$, defined by

$$dN_{at} = g(r) dr \quad (7)$$

where $dN_{at}(r)$ is the number of atoms at distances from the center of mass between r and $r + dr$.

III. RESULTS

A very important issue in the simulations of cluster melting is the election of the low-temperature isomer to be heated. A good knowledge of the ground state structure (global minimum) is required, as the details of the melting transition are known to be isomer-dependent.³⁰ But the problem of performing a realistic global optimization search is exponentially difficult as size increases, so finding the global minima of clusters with 55 atoms or more becomes impractical. In our previous work⁸ we directly started from icosahedral isomers for Na_{55} , Na_{92} and Na_{142} , as there is some experimental⁹ and theoretical³¹ indications that suggest icosahedral packing in sodium clusters, and found a good agreement with the experimental results of Haberland’s group.¹⁰ Simulated annealing runs for Na_{92} and Na_{142} always led to disordered structures with an energy higher than that of

the corresponding icosahedral isomer. The melting behavior of these disordered structures was analyzed separately and found to be different from that of icosahedral clusters.³² As the comparison with experiment was favourable only for icosahedral isomers and the total energy of these structures was always lower than that of disordered structures, we have chosen icosahedral isomers in the study of the melting behavior of large alkali clusters: K_{55} , Rb_{55} and Cs_{55} are complete two-shell icosahedrons, K_{92} and K_{142} are incomplete three-shell icosahedrons constructed by following the icosahedral growing pattern described by Montejano-Carrizales *et al.*³³ The low-temperature isomer of K_{20} was obtained by the dynamic simulated annealing technique,¹⁴ by heating the cluster to 400 K and then slowly reducing the temperature. The resulting structure is essentially the same as that obtained for Na_{20} with the same technique.⁷

The temperature evolutions of the specific heat C_v and of the rms bond length fluctuation δ of K_{20} are shown in Fig. 1. The specific heat displays two maxima around 90 K and 130 K. The $\delta(T)$ curve has a small positive slope at low temperatures that reflects the thermal expansion of the solidlike cluster, and then two abrupt increases that correlate with the two peaks in the specific heat. Both magnitudes indicate that the melting of K_{20} occurs in two well separated steps over a wide range of temperatures. To analyse the nature of those two steps we show in Fig. 2 short-time averages of the “atomic equivalence indexes” of K_{20} for a number of representative temperatures. For a temperature at which the cluster is completely solid, the $\sigma_i(t)$ curves show a high degeneracy which is specific of the symmetry of the isomer under consideration.³⁰ The structure of K_{20} , as that of Na_{20} ,⁷ can be divided into two subsets: two internal “core” atoms and 18 peripheral “surface” atoms. The transition at ≈ 90 K is identified with an isomerization transition in which the 18 peripheral atoms begin to interchange their positions in the cluster while the two central atoms remain oscillating around their initial positions. When a temperature of ≈ 130 K is reached, one of the two inner atoms moves out to the cluster surface, while the other remains in its central position. Then the second transition is identified with another isomerization transition in which a new set of (19+1) isomers begins to be visited. The δ quantity increases with temperature after this point in a smooth way. This is due to the more and more frequent interchanges of the central atom with one of the peripheral atoms upon increasing the temperature. Nevertheless, the interchange rate between central and peripheral atoms remains slower than the interchange rate between peripheral atoms for all temperatures considered.

Fig. 3 shows the specific heat and δ curves for K_{55} . The specific heat displays a main asymmetric peak centered approximately at 160 K, while δ shows two abrupt increases at ≈ 110 K and 160 K. The second abrupt increase in δ coincides with the position of the main specific heat peak. Although the first step in δ is not in correspondence with any well-defined specific heat peak,

there is a visible shoulder in the low temperature side (a clear asymmetry) of that peak. Moreover, the width of the transition region, approximately 100 K, is predicted to be the same with both indicators. The nature of melting is analyzed by plotting the temperature evolution of the time-averaged radial atomic density distribution $g(r)$. At a low temperature of $T=86$ K, Fig. 4 shows that the atoms are distributed in several icosahedral shells (in the outer shell, the twelve atoms in vertex positions can be distinguished from the rest due to slightly different radial distances). At the temperature where the first step in δ emerges, the detailed structure in the ionic density distribution has been washed out by the thermal effects, and the movies show that the cluster surface is melted. However, the different shells are still clearly distinguished, showing that there are not interchanges between atoms in different shells. At a temperature higher than 160 K, the distinction of the several radial shells is not possible anymore. All the atoms are able to diffuse across the cluster volume, that is both intrashell and intershell displacements are allowed, and the liquid phase is completely established. Upon a further increasing in temperature, the only appreciable change in $g(r)$ is due to the thermal expansion of the cluster.

The results for K_{92} are shown in Figs. 5 and 6. Both the specific heat and δ predict a two-step melting process, with a first transition at ≈ 110 K and a second transition at ≈ 200 K. As seen in Fig. 6, the first transition is associated again with surface melting, with no substantial intershell diffusion. For temperatures higher than 200 K, the cluster is completely liquid. K_{142} melts in two main steps, at ≈ 140 K and 230 K (Fig. 7). There is also a small bump on the low-temperature side of the first specific heat peak, correlated with a small abrupt increase of δ at ≈ 90 K. This previous step is associated with an isomerization regime in which different isomers preserving the icosahedral symmetry are visited, and was also found for Na_{142} .⁸ These isomerizations involve the motion of the five vacancies in the outer shell. The surface melting stage is not developed yet, however, as the icosahedral order persists. The distribution of atoms in three shells is still distinguished at a temperature of 190 K where the cluster surface is melted. The average radial ionic density distribution is not completely uniform until the homogeneous melting temperature is reached.

The bulk melting temperature of K (337 K)³⁴ is reduced by a 10 % with respect to that of Na (371 K).³⁴ The melting temperatures of K clusters are also smaller than those of Na clusters^{7,8} for all the sizes studied. The percentage reduction in melting temperature is substantially larger than in the bulk and a slightly decreasing function of cluster size (19 %, 17 %, 16 % and 15 % for $N=20, 55, 92,$ and $142,$ respectively). The nature of the several premelting effects observed are similar for both materials. Nevertheless, they are more easily established in the case of K clusters. For example, surface and homogeneous melting temperatures were closer together in the case of Na_{142} (240 K and 270 K, respectively)⁸ than

they are for K_{142} (140 K and 230 K, respectively); while two-step melting was not observed for a perfect two-shell Na_{55} icosahedron,⁸ the melting surface stage is well established for K_{55} , which has the same low-temperature structure; in general, the transition region is wider for K than for Na clusters.

As the main points in this comparison are quite independent of cluster size, we analyze in the following the melting behavior of Rb and Cs clusters for a fixed cluster size, namely $N=55$. Specific heat and δ curves as a function of temperature are given in Figs. 9 and 10. The results are similar to those obtained for K_{55} , namely a main asymmetric specific heat peak and two steps in δ , the last of which correlates with the peak in the specific heat. The radial ionic density distributions of both materials present a similar temperature dependence and only the results for Cs_{55} are shown in Fig. 11. The first transition (at ≈ 110 K for Rb_{55} and ≈ 90 K for Cs_{55}) is identified with surface melting: Fig. 11 at 110 K shows that inter-shell diffusion is not important yet. The second (at ≈ 140 K for Rb_{55} and 130 K for Cs_{55}) corresponds to homogeneous melting. We find that the different alkali clusters with $N=55$ atoms melt in a similar way. The main differences are the following: a) The homogeneous melting temperature decreases with increasing atomic number as in the bulk case, but in a more pronounced way. Specifically, in the series $Na \rightarrow K \rightarrow Rb \rightarrow Cs$, the bulk melting temperatures decrease by percentage values of 10 %, 7 %, and 3 %, respectively,³⁴ while for the 55-atom clusters the corresponding percentage values are 17 %, 12.5 %, and 7 %, respectively; b) The height of the specific heat peaks decreases and their width increases with increasing atomic number; c) Premelting effects are more important for the heavier elements. Specifically, two-step melting was not observed in the case of Na_{55} ,⁸ while a well defined surface melting stage is observed in the thermal evolution of K_{55} , Rb_{55} and Cs_{55} .

It is perhaps not surprising that the melting temperature reduction is larger in clusters compared to the bulk phase, where coordination effects associated with a large proportion of atoms in surface-like positions do not appear. But a meaningful comparison can not be done due to the different structures adopted by alkali elements in the cluster (icosahedral packing) and bulk (bcc packing) phases. The other two points do not invoke any comparison with the bulk phase, and can be more conveniently addressed. Rey *at al.*³⁵ have analyzed the influence of the softness of the repulsive core interaction on cluster melting. Specifically, a series of pair potentials differing just in their shape in the core region was constructed and used to investigate the melting behavior of 13-particle clusters. For those potentials with soft core repulsion, two-step melting was observed: the first step corresponds to the onset of frequent isomerizations involving only the surface atoms, while the second corresponds to homogeneous melting, involving also the central atom. For the harder potentials, those two steps merge into one, and melting-in-steps processes do not ap-

pear. The repulsive part of our pseudopotential is harder the lighter is the alkali element,²⁶ so the importance of premelting effects can be expected to increase in the series $Na \rightarrow K \rightarrow Rb \rightarrow Cs$. In effect, a well-defined surface melting stage is not observed for Na_{55} , while it develops before the homogeneous melting point for the heavier alkali elements. Moseler and Nordiek³⁶ have studied the influence of the potential range on the heat capacity of 13-atom Morse clusters. They have found that decreasing the range of the potential increases the peak of the heat capacity in the melting transition region. The range of our pseudopotential increases with atomic number for the alkali elements,²⁶ so a decrease in the height of the specific heat peak is expected in the series $Na \rightarrow K \rightarrow Rb \rightarrow Cs$. This is what is observed indeed. Thus, we conclude that melting proceeds in a qualitatively similar way in clusters of the alkali elements Na, K, Rb and Cs, and that the small existing differences can be explained in terms of the different parameters defining the corresponding local pseudopotentials.

A few comments regarding the quality of the simulations and of the annealing runs are perhaps in order here. The orbital-free representation of the atomic interactions is much more efficient than the more accurate KS treatments, but is still substantially more expensive computationally than a simulation using phenomenological many-body potentials. Such potentials contain a number of parameters that are usually chosen by fitting some bulk and/or molecular properties. In contrast our model is free of external parameters, although there are approximations in the kinetic and exchange-correlation functionals. The orbital-free scheme accounts, albeit approximately, for the effects of the detailed electronic distribution on the total energy and the forces on the ions. We feel that this is particularly important in metallic clusters for which a large proportion of atoms are on the surface and experience a very different electronic environment than an atom in the interior. Furthermore, the adjustment of the electronic structure and consequently the energy and forces to rearrangements of the ions is also taken into account. But the price to be paid for the more accurate description of the interactions is a less complete statistical sampling of the phase space. The simulation times are substantially shorter than those that can be achieved in phenomenological simulations. Nevertheless, we expect that the locations of the several transitions are reliable, because all the indicators we have used, both thermal and structural ones, are in essential agreement on the temperature at which the transitions start.

IV. SUMMARY

The melting-like transition in K_N , with $N=20, 55, 92$ and 142, Rb_{55} and Cs_{55} clusters has been investigated by applying an orbital-free, density-functional molecular dynamics method. The computational effort which

is required is modest in comparison with the traditional Car-Parrinello Molecular Dynamics technique based on Kohn-Sham orbitals, that would be very costly for clusters of these sizes. The details of the several transitions have been explained and found to be similar to those found in the melting-like transition of sodium clusters:^{7,8} alkali clusters show generally a separate surface melting stage prior to homogeneous melting. The homogeneous melting temperature has been found to decrease with increasing atomic number as in the bulk limit, but the percentage value of this temperature reduction is larger than for the bulk materials, due to the larger proportion of surface-like atoms existing in the cluster; in fact, the reduction in melting temperature when passing from Na to K clusters slightly decreases with increasing cluster size. The height of the specific heat peaks decreases and their width increases with increasing atomic number, and the premelting effects are more important for the heavier alkalis. These trends have been rationalized in terms of physical features of the local pseudopotentials employed.

ACKNOWLEDGMENTS: This work has been supported by DGES (Grant PB98-0368) and Junta de Castilla y León (VA70/99). The author acknowledges useful discussions with J. M. López.

Captions of Figures.

Figure 1 Specific heat (a) and δ (b) curves of K_{20} , taking the internal cluster temperature as the independent variable. The deviation around the mean temperature is smaller than the size of the circles.

Figure 2 Short-time averaged distances $\langle r_i(t) \rangle_{sta}$ between each atom and the center of mass in K_{20} , as functions of time for four representative values of the internal temperature. The bold lines follow the evolution of particular atoms.

Figure 3 Specific heat (a) and δ (b) curves of K_{55} , taking the internal cluster temperature as the independent variable. The deviation around the mean temperature is smaller than the size of the circles.

Figure 4 Time averaged radial atomic density distribution of K_{55} , at four representative temperatures.

Figure 5 Specific heat (a) and δ (b) curves of K_{92} , taking the internal cluster temperature as the independent variable. The deviation around the mean temperature is smaller than the size of the circles.

Figure 6 Time averaged radial atomic density distribution of K_{92} , at four representative temperatures.

Figure 7 Specific heat (a) and δ (b) curves of K_{142} , taking the internal cluster temperature as the independent variable. The deviation around the mean temperature is smaller than the size of the circles.

Figure 8 Time averaged radial atomic density distribution of K_{142} , at four representative temperatures.

Figure 9 Specific heat (a) and δ (b) curves of Rb_{55} , taking the internal cluster temperature as the independent

variable. The deviation around the mean temperature is smaller than the size of the circles.

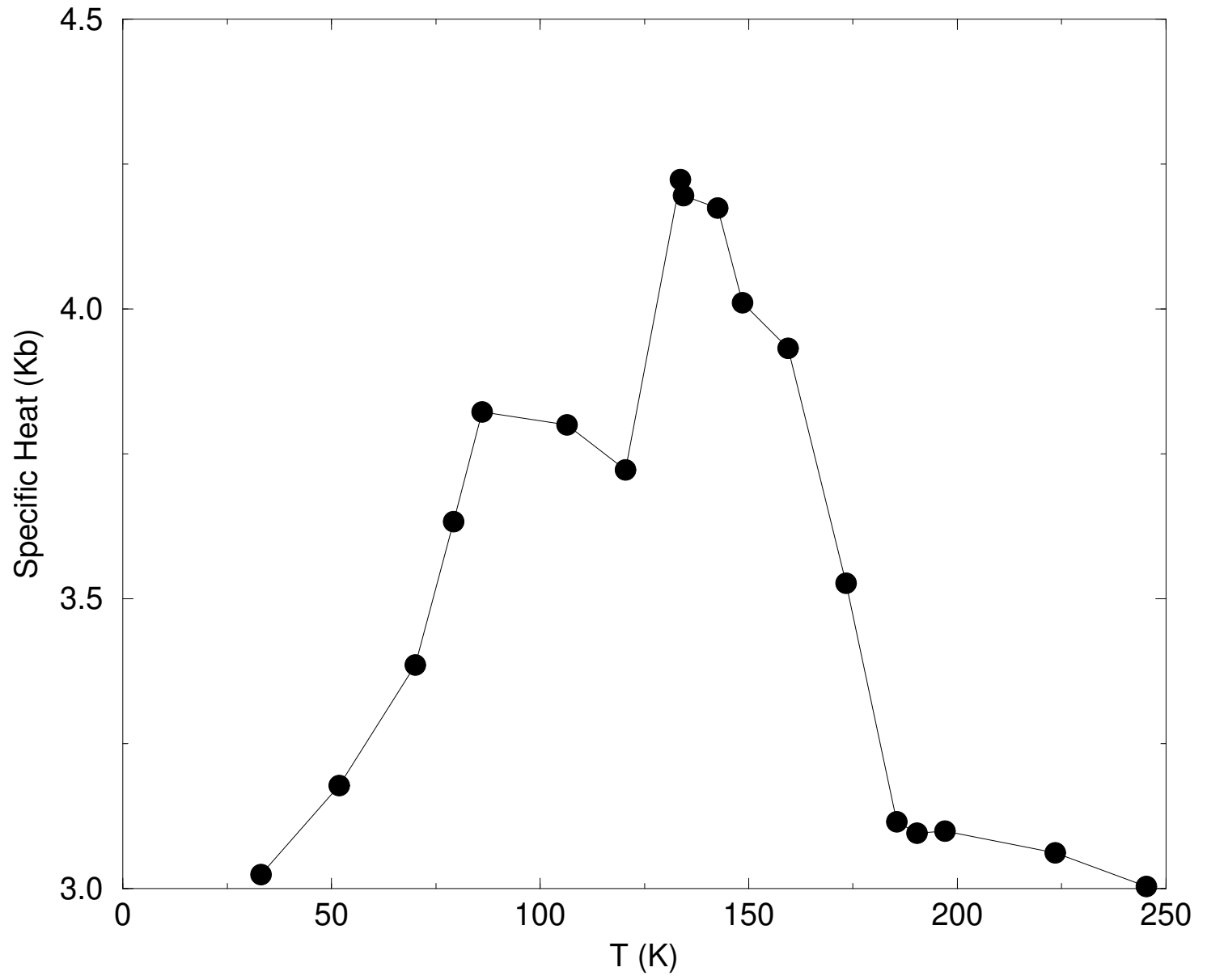
Figure 10 Specific heat (a) and δ (b) curves of Cs_{55} , taking the internal cluster temperature as the independent variable. The deviation around the mean temperature is smaller than the size of the circles.

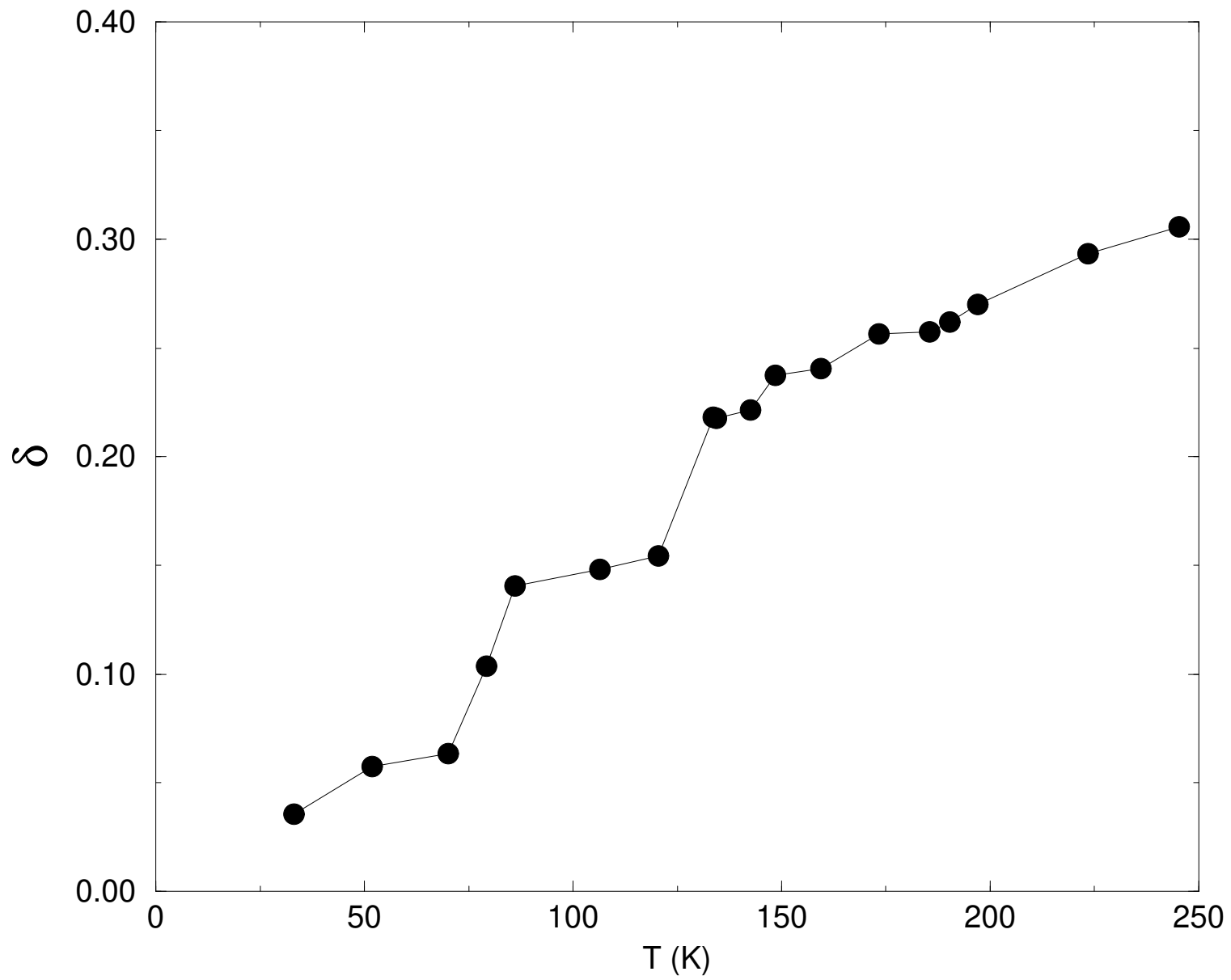
Figure 11 Time averaged radial atomic density distribution of Cs_{55} , at four representative temperatures.

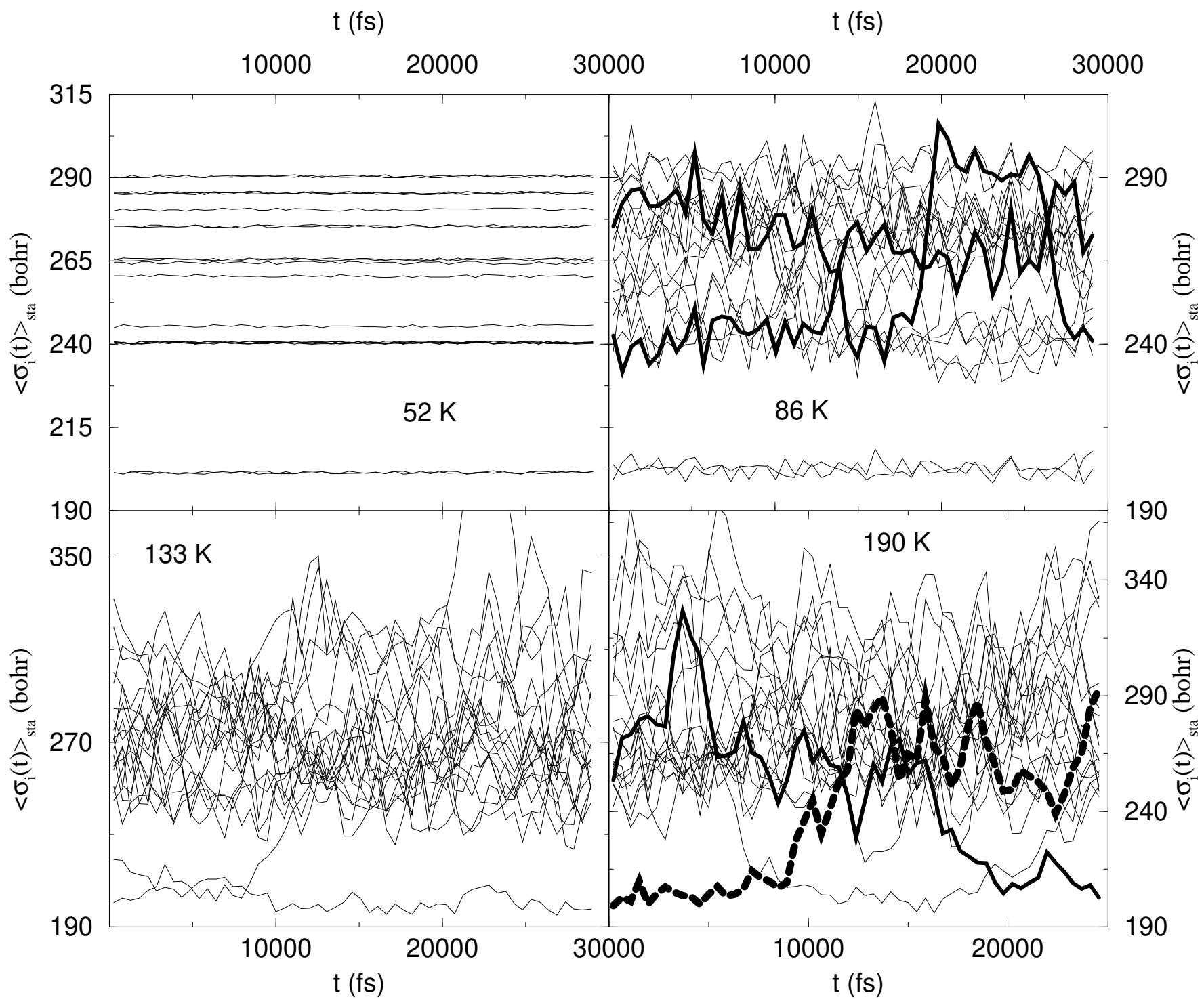
-
- ¹ J. Jellinek, T. L. Beck, and R. S. Berry, *J. Chem. Phys.* **84**, 2783 (1986); H. L. Davis, J. Jellinek, and R. S. Berry, *ibid.* **86**, 6456 (1987); T. L. Beck, J. Jellinek, and R. S. Berry, *ibid.* **87**, 545 (1987); H. P. Cheng and R. S. Berry, *Phys. Rev. A* **45**, 7969 (1991); J. P. Rose and R. S. Berry, *ibid.* **96**, 517 (1992); *ibid.* **98**, 3246 (1993); *ibid.* **98**, 3262 (1993); Z. B. Güvenc and J. Jellinek, *Z. Phys. D* **26**, 304 (1993); V. K. W. Cheng, J. P. Rose, and R. S. Berry, *Surf. Rev. Lett.* **3**, 347 (1996).
 - ² A. Bulgac and D. Kusnezov, *Phys. Rev. Lett.* **68**, 1335 (1992); *Phys. Rev. B* **45**, 1988 (1992); N. Ju and A. Bulgac, *Phys. Rev. B* **48**, 2721 (1993); M. Fosmire and A. Bulgac, *ibid.* **52**, 17509 (1995); J. M. Thompson and A. Bulgac, *ibid.* **40**, 462 (1997); L. J. Lewis, P. Jensen, and J. L. Barrat, *ibid.* **56**, 2248 (1997); S. K. Nayak, S. N. Khanna, B. K. Rao, and P. Jena, *J. Phys.: Condens. Matter* **10**, 10853 (1998). F. Calvo and P. Labastie, *J. Phys. Chem. B* **102**, 2051 (1998); J. P. K. Doye and D. J. Wales, *Phys. Rev. B* **59**, 2292 (1999); *J. Chem. Phys.* **111**, 11070 (1999).
 - ³ P. Blaise, S. A. Blundell, and C. Guet, *Phys. Rev. B* **55**, 15856 (1997).
 - ⁴ A. Rytönen, H. Häkkinen, and M. Manninen, *Phys. Rev. Lett.* **80**, 3940 (1998).
 - ⁵ C. L. Cleveland, W. D. Luedtke, and U. Landman, *Phys. Rev. Lett.* **81**, 2036 (1998); *Phys. Rev. B* **60**, 5065 (1999).
 - ⁶ F. Calvo and F. Spiegelmann, *Phys. Rev. Lett.* **82**, 2270 (1999); *J. Chem. Phys.* **112**, 2888 (2000).
 - ⁷ A. Aguado, J. M. López, J. A. Alonso, and M. J. Stott, *J. Chem. Phys.* **111**, 6026 (1999).
 - ⁸ A. Aguado, J. M. López, J. A. Alonso, and M. J. Stott, *J. Phys. Chem. B*, submitted (preprint available at <http://xxx.lanl.gov/abs/physics/9911042>).
 - ⁹ T. P. Martin, *Phys. Rep.* **273**, 199 (1996).
 - ¹⁰ M. Schmidt, R. Kusche, W. Kronmüller, B. von Issendorff, and H. Haberland, *Phys. Rev. Lett.* **79**, 99 (1997); M. Schmidt, R. Kusche, B. von Issendorff, and H. Haberland, *Nature* **393**, 238 (1998); R. Kusche, Th. Hippler, M. Schmidt, B. von Issendorff, and H. Haberland, *Eur. Phys. J. D* **9**, 1 (1999).
 - ¹¹ M. Schmidt, C. Ellert, W. Kronmüller, and H. Haberland, *Phys. Rev. B* **59**, 10970 (1999).
 - ¹² H. Haberland, in *"Metal Clusters"*, ed. W. Ekardt (John Wiley & Sons, 1999), p. 181.
 - ¹³ M. Pearson, E. Smargiassi, and P. A. Madden, *J. Phys.: Condens. Matter* **5**, 3221 (1993).
 - ¹⁴ R. Car and M. Parrinello, *Phys. Rev. Lett.* **55**, 2471 (1985);

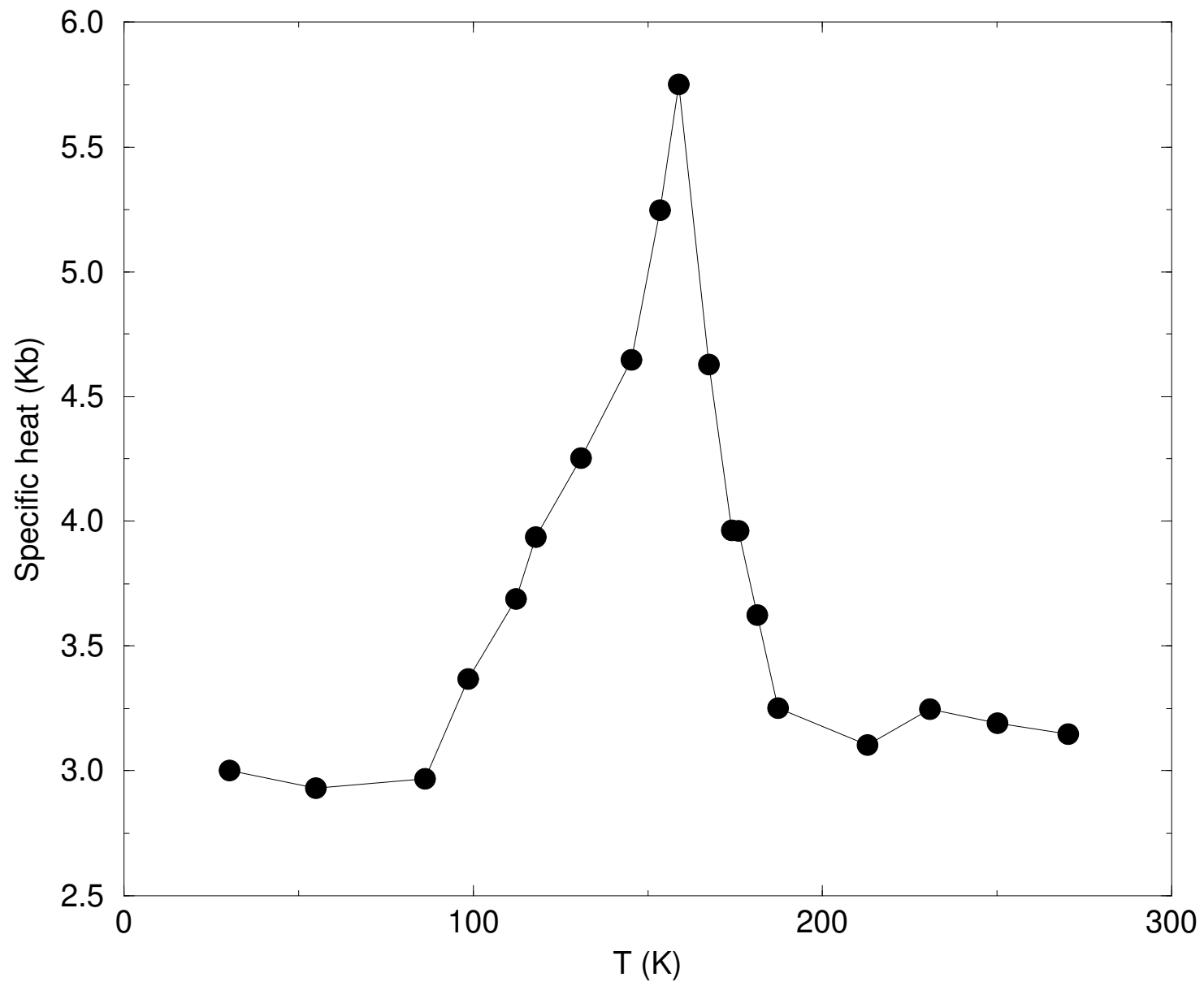
- M. C. Payne, M. P. Teter, D. C. Allan, T. A. Arias, and J. D. Joannopoulos, *Rev. Mod. Phys.* **64**, 1045 (1992).
- ¹⁵ P. Hohenberg and W. Kohn, *Phys. Rev.* **136**, 864B (1964).
- ¹⁶ W. Kohn and L. J. Sham, *Phys. Rev.* **140**, 1133A (1965).
- ¹⁷ E. Smargiassi and P. A. Madden, *Phys. Rev. B* **49**, 5220 (1994); M. Foley, E. Smargiassi, and P. A. Madden, *J. Phys.: Condens. Matter* **6**, 5231 (1994); E. Smargiassi and P. A. Madden, *Phys. Rev. B* **51**, 117 (1995); *ibid.* **51**, 129 (1995); M. Foley and P. A. Madden, *ibid.* **53**, 10589 (1996); B. J. Jesson, M. Foley, and P. A. Madden, *ibid.* **55**, 4941 (1997); J. A. Anta, B. J. Jesson, and P. A. Madden, *ibid.* **58**, 6124 (1998).
- ¹⁸ N. Govind, Y. A. Wang, and E. A. Carter, *J. Chem. Phys.* **110**, 7677 (1999).
- ¹⁹ V. Shah, D. Nehete, and D. G. Kanhere, *J. Phys.: Condens. Matter* **6**, 10773 (1994); D. Nehete, V. Shah, and D. G. Kanhere, *Phys. Rev. B* **53**, 2126 (1996); V. Shah and D. G. Kanhere, *J. Phys.: Condens. Matter* **8**, L253 (1996); V. Shah, D. G. Kanhere, C. Majumber, and G. P. Das, *ibid.* **9**, 2165 (1997); A. Vichare and D. G. Kanhere, *J. Phys.: Condens. Matter* **10**, 3309 (1998); A. Vichare and D. G. Kanhere, *Eur. Phys. J. D* **4**, 89 (1998); A. Dhavale, V. Shah, and D. G. Kanhere, *Phys. Rev. A* **57**, 4522 (1998).
- ²⁰ N. Govind, J. L. Mozos, and H. Guo, *Phys. Rev. B* **51**, 7101 (1995); Y. A. Wang, N. Govind, and E. A. Carter, *ibid.* **58**, 13465 (1998).
- ²¹ *Theory of the inhomogeneous electron gas*. Editors S. Lundqvist and N. H. March. Plenum Press, New York (1983).
- ²² W. Yang, *Phys. Rev. A* **34**, 4575 (1986).
- ²³ J. P. Perdew, *Phys. Lett. A* **165**, 79 (1992).
- ²⁴ J. P. Perdew and A. Zunger, *Phys. Rev. B* **23**, 5048 (1981).
- ²⁵ D. Ceperley and B. Alder, *Phys. Rev. Lett.* **45**, 566 (1980).
- ²⁶ C. Fiolhais, J. P. Perdew, S. Q. Armster, J. M. McLaren, and H. Brajczewska, *Phys. Rev. B* **51**, 14001 (1995); *ibid.* **53**, 13193 (1996); *ibid.* **59**, 2570 (1999).
- ²⁷ F. Nogueira, C. Fiolhais, J. He, J. P. Perdew, and A. Rubio, *J. Phys.: Condens. Matter* **8**, 287 (1996).
- ²⁸ L. Verlet, *Phys. Rev.* **159**, 98 (1967); W. C. Swope and H. C. Andersen, *J. Chem. Phys.* **76**, 637 (1982).
- ²⁹ S. Sugano, *Microcluster Physics*, Springer-Verlag, Berlin (1991).
- ³⁰ V. Bonacić-Koutecký, J. Jellinek, M. Wiechert, and P. Fantucci, *J. Chem. Phys.* **107**, 6321 (1997); D. Reichardt, V. Bonacić-Koutecký, P. Fantucci, and J. Jellinek, *Chem. Phys. Lett.* **279**, 129 (1997).
- ³¹ S. Kümmel, P. -G. Reinhard, and M. Brack, *Eur. Phys. J. D* **9**, 149 (1999); S. Kümmel, M. Brack, and P. -G. Reinhard, unpublished results.
- ³² A. Aguado, unpublished results.
- ³³ J. M. Montejano-Carrizales, M. P. Iñiguez, J. A. Alonso, and M. J. López, *Phys. Rev. B* **54**, 5961 (1996).
- ³⁴ N. M. Ashcroft and N. D. Mermin, *Solid State Physics*, Holt, Rinehart and Winston, New York (1976).
- ³⁵ C. Rey, J. García-Rodeja, L. J. Gallego, and M. J. Grimson, *ibid.* **57**, 4420 (1998).
- ³⁶ M. Moseler and J. Nordiek, *Phys. Rev. B* **60**, 11734 (1999).

2









11

